

Non-uniform Feeding Network for a Dual Circularly Polarized 16×16 Ku-Band Antenna Array for On-Move Satellite Communication

W. M. Hassan¹, Khalid M. Ibrahim¹, E. A. Abdallah², and A. M. Attiya¹

¹Microwave Engineering Department
Electronics Research Institute (ERI), El-Nozha El-Gadidah, Cairo, 11843 Egypt
walaa81hassan@yahoo.com, khaledmus@gmail.com, attiya@eri.sci.eg

²Microstrip Department
Electronics Research Institute (ERI), El-Nozha El-Gadidah, Cairo, 11843 Egypt
esmataa2@hotmail.com

Abstract – This paper presents analysis and design of a dual circularly polarized 16×16 Ku band antenna array with emphasis on its feeding network. The proposed antenna is designed for on-move satellite communication system where the radiation pattern and the side-lobe level should meet the ITU standards to avoid interference with other satellite systems. This requirement is obtained by using non-uniform feeding distribution network. In addition, dual circular polarization operation requires sequential feeding networks with appropriate phase shift sequences. The proposed antenna is divided into 16 sub-cells of 4×4 radiating elements. The elements inside the sub-cell are fed by uniform dual sequential feeding networks. These sub-cells are connected together via two non-uniform feeding networks on a single layer in the shape of two interlaced fork configurations. In addition, cascaded power dividers are used to achieve the required low power division ratios between some of the sub-cells according to the required feeding distribution. These modifications simplify the fabrication process of the proposed antenna structure and reduce the required layers while satisfying the required radiation parameters.

Index Terms – Antenna array, circular polarized antenna, feeding network, Ku-band antenna, satellite antenna.

I. INTRODUCTION

On-move Ku-band satellite communication systems have a significant importance in different military and civilian applications where it may not be available other wired or wireless communication systems. This situation can usually be found in rural areas, in deserts, in ships away from shores and other similar situations. Parabolic reflector antennas with horn feeding are good candidate for fixed transceiver systems. However, for the case of moving situations like cars, trains and ships, the size and the aerodynamics of reflector antennas may not be suitable for these applications. In these cases, a planar

antennas inside a radom represent a better choice for antenna structure than reflector antenna. The suitable planar antenna for such application usually has the configuration of an antenna array. Different planar antenna arrays for satellite communication systems were developed in X band and Ku band. The type of the radiating element and the feeding networks of such antenna arrays represent the main design parameters. On the other hand, the operating bandwidth, the radiation pattern, and the polarization represent some of the main specifications which should be included in the proposed antenna design. In addition, the weight, the manufacturing process and the number of layers represent important aspects in developing these antenna arrays.

In this paper we present a dually circular polarized antenna array operating in Ku band in the frequency range from 10.5 to 14.5 GHz. The proposed antenna array is composed of 4×4 sub-cells where each sub-cell is composed of 4×4 radiating elements. Each radiating element is fed by wideband branch-line coupler to introduce dually circular polarization. Each 2×2 radiating elements are connected by dual sequential feeding networks for both circular polarizations [1]. These 2×2 sequential fed elements are connected by uniform feeding networks to compose the sub-cells composed of 4×4 radiating elements. To develop a total radiation pattern compatible with the required ITU standards for satellite communication systems [2], these sub-cells are connected by dual non-uniform feeding networks for both polarizations [3]. The distributions of these feeding networks have a significant effect on the error function between the obtained radiation pattern and the standard ITU Mask. On the other hand, developing such distribution function may require developing complicated power dividers with quite small power division ratios. In addition, integrating the dual non-uniform feeding networks on a single layer to reduce the number of layers in the designed antenna represents another critical aspect

in the proposed design.

Similar antenna configurations can be found in literature. However, not all the previously mentioned specifications are found in these configurations. In [4] a LH circularly polarized slot antenna array is presented in the frequency range from 12.01 to 12.14 GHz with a uniform SIW feeding network. Another configuration is presented in [5] based on sequentially fed microstrip patches fed by a SIW feeding network to operate in the frequency range from 11.55 to 12.25 GHz with LH circular polarization. A dual band dual circularly polarized array is presented in [6] based on two layers of different polarization rotation artificial magnetic conductor operating at different frequency bands. The two bands in this case are 8.15 to 8.35 GHz for RH circular polarization and 14.2 to 14.8 GHz for LH circular polarization. Uniform feeding distribution function is used to feed the exciting double sided dipole array. On the other hand, other similar configurations are discussed in other frequency bands. A ridge gap waveguide feeding network is discussed to feed a RH circularly polarized array in mm-wave range [7]. A dual circularly polarized antenna based on slotted SIW is presented in [8] with a bandwidth extends from 11.6 to 13 GHz. Other configurations based on dual linearly polarized antenna arrays in Ku band are also discussed in [9 – 11]. In these configurations waveguide feeding networks with complicated manufacturing process were used.

On the other hand, similar antenna structures are studied in X-band [12 – 14]. In [12] the main feeding networks is implemented by using corporate feeding networks on two different layers separated by a ground plane to implement the dual circular polarizations. However, in [13] these feeding networks are implemented on the same layer, but for smaller antenna array. Based on the results shown in [3], the feeding distribution function used in [12 – 13] are not the optimum to reduce the error with respect to the ITU mask. However, better distribution functions would require less power division ratios which are more complicated in physical implementation. This is the motivation here to introduce a new non-uniform feeding network which can be interlaced with another similar one on the same layer to feed dual polarized 4×4 sub-cells in Ku-band. This dual non-uniform feeding network is used to develop 16×16 dual circularly polarized antenna array in Ku band in the frequency range from 10.5 to 14.5 GHz.

The organization of the present paper is as follows: In Sec. II we present in detail the geometry of the radiating element with its feeding network to introduce dual circular polarization. Then we introduce the designed dual sequential feeding networks for the sub-cell. The main properties for the sub-cell is given. In Sec. III, we

present the analysis and design of the proposed non-uniform feeding network which connect these sub-cells to compose the proposed 16×16 antenna array. In this section the main limits on implementing this non-uniform feeding networks and how it can be implemented by using cascaded power divider are given. In addition, we present in this section how to integrate the two feeding networks for the two polarizations on the same layer. Section IV presents the experimental results for the designed antenna array. Finally, Sec. V gives the conclusion.

II. SEQUENTIAL FEEDING NETWORK FOR DUAL CIRCULAR POLARIZED 4×4 ANTENNA ARRAY

The proposed antenna array is composed of 4×4 sub-cells. Each sub-cell is composed of a 4×4 antenna array. Different configurations for radiating elements can be used of this application [15 – 17]. However, in the present case, it is required to develop a wideband antenna element with dual circular polarization. The appropriate configuration in this case is a stacked symmetric microstrip patch fed by a wideband branch-line coupler [13], [18], and [22].

The used radiating element in the present case is a stacked circular patch microstrip antenna as shown in Fig. 1. The lower fed element is printed on a substrate RT/duroid 5880 with substrate thickness $L_2 = 0.787$ mm. The dielectric constant of RT/duroid 5880 is 2.2 and loss tangent is 0.0009. On the other hand, the upper parasitic element is printed on a substrate RO3003 with substrate thickness $L_1 = 0.25$ mm. The dielectric constant of RO3003 is 3 and loss tangent is 0.001. The parasitic element is separated from the fed element by a foam layer of thickness $L_F = 2$ mm. The radius of the lower patch is 8.2 mm and the radius of the upper patch is 8.8 mm. This stacked configuration is designed to verify the required wideband operation of the proposed antenna in the frequency range from 10.5 to 14.5 GHz. This antenna element is fed by two feeding probes through vias which are connected in a separate layer by a wideband branch line-coupler (BLC) to introduce the required dual circular polarizations. The dimensions of the BLC are $L_4 = 4.95$ mm, $L_6 = 1.2$ mm, $T_2 = 0.3$ mm, $T_3 = 0.6$ mm, and $T = 0.9$ mm as shown in Fig.1(c). The feeding BLC is printed on a substrate RO3003 with thickness $L_3 = 0.25$ mm. These radiating elements are arranged in 2×2 configurations. The separation between the elements is 18 mm which is nearly $0.75\lambda_0$ at the center frequency. This 2×2 antenna array is fed by two interlaced sequential feeding networks with two opposite sequences to compose dual circularly polarized 2×2 antenna array.

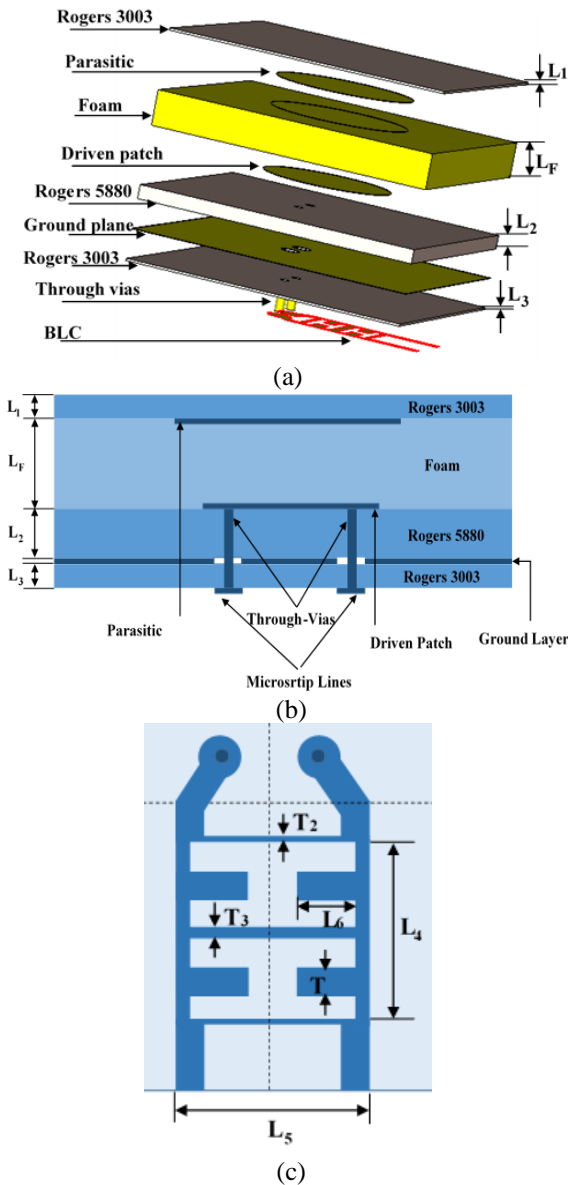


Fig. 1. Geometry of the radiating element of the antenna array: (a) 3-D view, (b) side view, and (c) BLC.

This sequential feeding networks include successive phase shifts of -90° in clockwise and counter clockwise directions to assets right hand and left hand circular polarizations, respectively. These successive phase shifts are obtained by increasing the feeding line sections by $\lambda_g/4$ in a successive form where λ_g is the guided wavelength of the feeding microstrip line on the feeding substrate. These $\lambda_g/4$ increments cannot be added directly in the form of straight lines due to the limited space between the radiating elements. Thus, multiple bends, U-shapes and meander shapes are used as shown in Fig. 2.

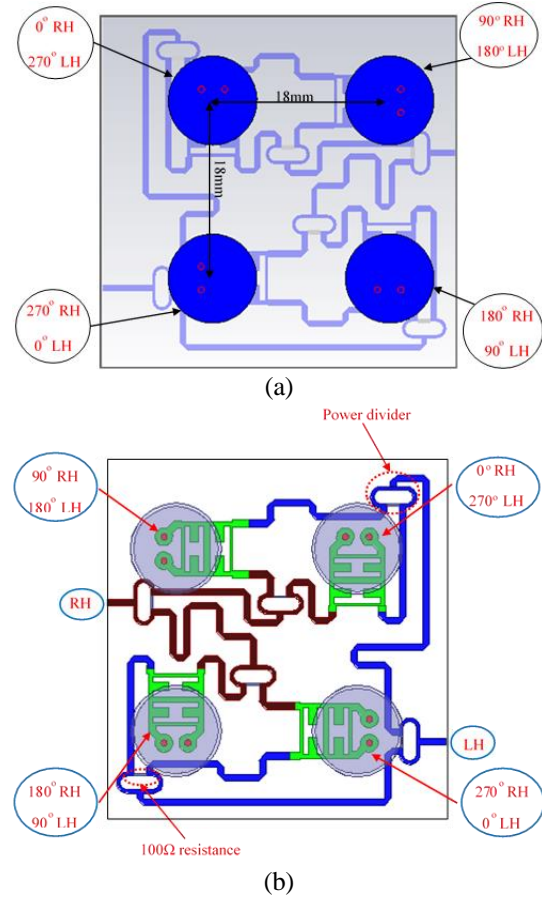


Fig. 2. Sequential feeding network for dual circularly polarized 2×2 radiating elements: (a) front view and (b) bottom view.

These configurations have additional effects in the total matching and phase sequence. In addition the coupling between the nearby sections of these feeding lines has additional effects. Thus, a preliminarily design of these two interlaced sequential feeding networks is obtained by using Keysight Advanced Design System (ADS2019). Then, this design is simulated by using full wave analysis Ansoft HFSS to include the effects of these parameters. This full wave analysis is optimized to introduce reflection coefficients below -10 dB and axial ratios below 3dB for the two circular polarizations in the operating band from 10.5 to 14.5 GHz [19]. Then, these 2×2 antenna arrays are arranged to compose the 4×4 sub-cell as shown in Fig. 3. In this case, the 2×2 arrays are connected together by two uniform interlaced feeding networks with equal amplitude and phase distribution. The total dimension of the sub-cell is 72×72 mm². To develop these uniform feeding networks in the available space, similar effects like bending and coupling should also be treated as in the case of the sequential feeding

networks of the 2×2 antenna array. In addition, to compensate the effects of mutual coupling between the nearby transmission line sections two matching stubs are added as shown in Fig. 3. The lengths of these matching stubs are optimized for both matching and axial ratio [19]. Figure 4 shows the fabricated 4×4 sub-cell.

Figure 5 shows the simulated and measured reflection coefficients of the two feeding ports of this sub-cell. It can be noted that the obtained reflection coefficients is below -10dB in almost all the entire operating bandwidth. On the other hand, Fig. 6 shows the corresponding axial ratios and gain for both RH and LH circular polarizations. It can be noted that the condition of axial ratio below 3 dB is verified in most of the operating bandwidth. The normalized radiation pattern of the sub-cell for both RH and LH circular polarization at 12.7 GHz is shown in Fig. 7. This sub-cell is the building block of the proposed 16×16 antenna array.

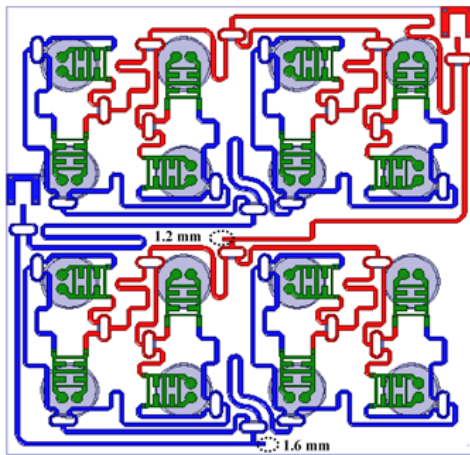


Fig. 3. Sequential feeding network with adjusting stubs for dual circularly polarized 4×4 radiating elements.

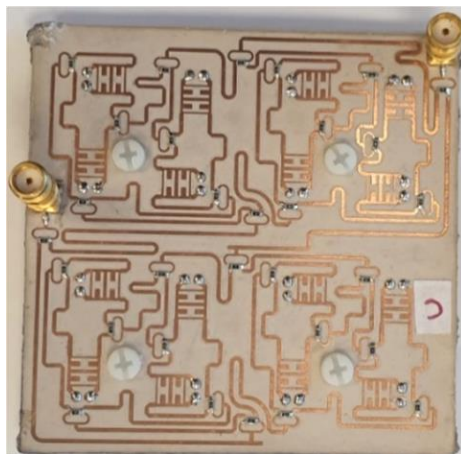


Fig. 4. Fabricated 4×4 sequential fed antenna (bottom side).

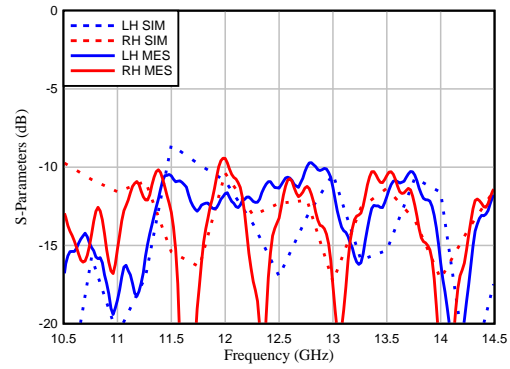


Fig. 5. Measured and simulated reflection coefficients of the 4×4 sequential fed antenna for LH and RH circular polarizations.

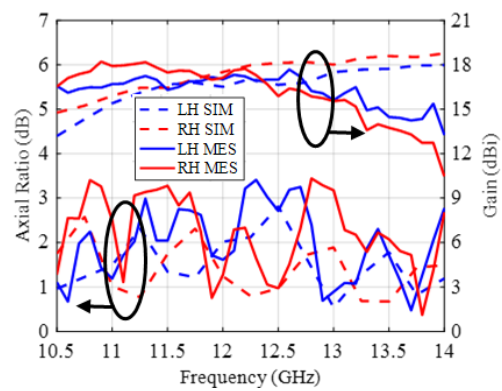
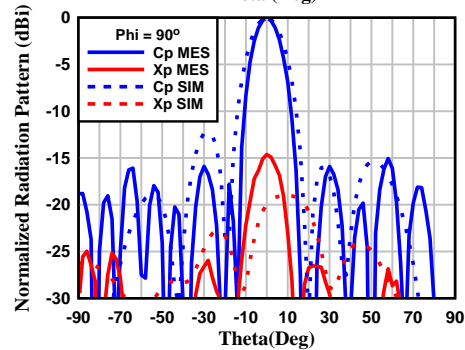
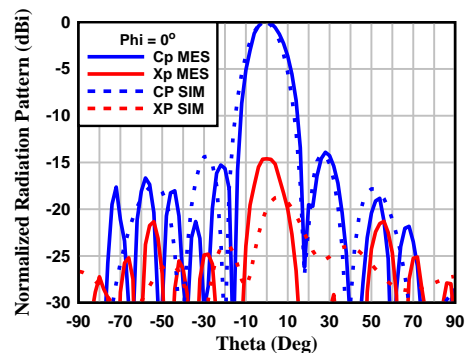


Fig. 6. Measured and simulated axial ratios and gain for RH and LH circular polarizations at broadside direction.



(a)

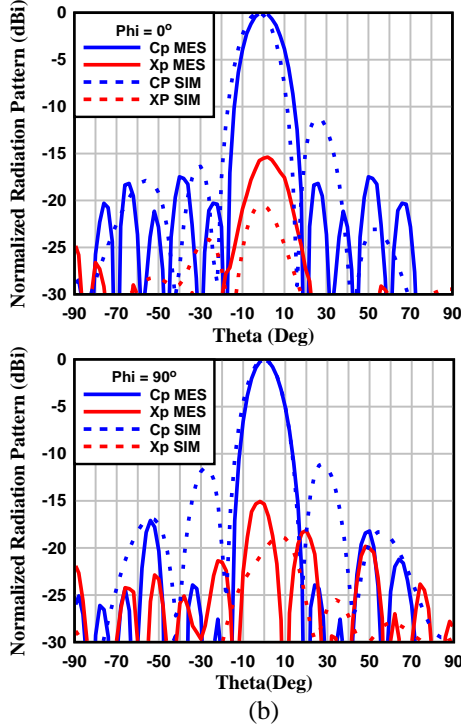


Fig. 7. Measured and simulation normalized radiation patterns for circular polarizations at 12.7 GHz (a) RH and (b) LH.

III. DESIGN AND ANALYSIS OF NON-UNIFORM FEEDING NETWORK FOR SUB-CELLS

The following step is to design a non-uniform feeding network to connect these sub-cells to form a 16×16 antenna array. Since the required radiation pattern is symmetric, the feeding distribution network should be symmetric as shown in Fig. 8, where A, B and C represent the amplitudes of the feeding current excitations at the different subcells. The amplitude A is normalized to be unity while B and C is less than unity. The total radiation pattern is a function of this distribution function and the radiation pattern of the sub-cell. The error function between the total radiation pattern and the required ITU Mask is defined as [3]:

$$\zeta = \frac{1}{N} \sum_i \frac{1 + \text{sgn}(P_r(\theta_i)_{\text{dBi}} - \text{Mask}(\theta_i)_{\text{dBi}})}{2} [P_r(\theta_i)_{\text{dBi}} - \text{Mask}(\theta_i)_{\text{dBi}}]. \quad (1)$$

For the case of a uniform distribution function along the array elements the error function is nearly 2 dBi.

Different configurations for distribution networks were discussed in [3] including continuous amplitude distributions, continuous phase distribution, complex distribution and complex distribution with discrete amplitudes. In the present case, continuous amplitude distribution is used to implement the required non-uniform feeding network. Thus, all the sub-cells have the

same phase. The error function between the ITU Mask and the total radiation pattern as a function of the amplitude distribution is shown in Fig. 9, assuming that the amplitude of the central sub-cells $A = 1$. It can be noted that the minimum error between the ITU Mask and the total radiation pattern can be obtained when $C \approx 0.6$ and $B < 0.4$. Previous implementations of similar feeding networks were based on distribution values $B = 0.8$ and $C = 0.6$. However, these values correspond to an error value much greater than the minimum value as shown in Fig. 9, where the error function in this case is around 1.53 dBi.

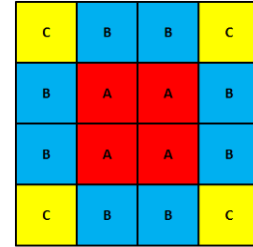


Fig. 8. Symmetric distribution function of a 16x16 array (Each square consists of 4x4 sub-cell).

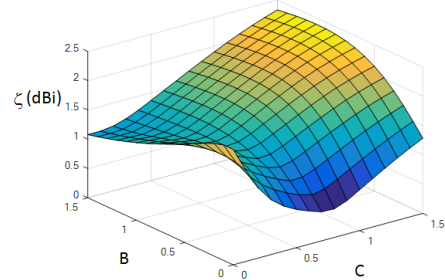


Fig. 9. Error w.r.t the ITU Mask as a function of B and C. The value of A is fixed to unity.

The key point in implementing these feeding distribution networks is the dimensions of the power dividers. These dimensions depend on the required characteristic impedances of the different transmission line sections of these power divider. For the case of a Wilkinson power divider with a non-equal power division ratio $P_3/P_2 = |V_3/V_2|^2 = K$, the required transmission line section of the power divider would have characteristic impedances of [20]:

$$Z_{03} = Z_0 \sqrt{\frac{1+K}{K^{3/2}}}, \quad (2-a)$$

$$Z_{02} = Z_0 \sqrt{K^{0.5}(1+K)}. \quad (2-b)$$

while the matching resistance between the two arms of the Wilkinson power divider is given by:

$$R = Z_0(\sqrt{K} + 1/\sqrt{K}). \quad (2-c)$$

In this case, the output ports 2 and 3 of the Wilkinson power divider are matched to impedances $Z_0\sqrt{K}$ and Z_0/\sqrt{K} , respectively. Thus, it would be required to add $\lambda_g/4$ transformer sections of impedances $Z_0K^{1/4}$ and $Z_0K^{-1/4}$, respectively to match the non-equal Wilkinson power divider to Z_0 load. For the case of a power ratio $K = 0.43$, the required impedance of Z_{03} would be nearly $2.25Z_0$. The feeding substrate is RO3003 with a dielectric constant $\epsilon_r = 3$ and substrate thickness $h = 0.25$ mm. The matching impedance $Z_0 = 50\Omega$. Thus, the required characteristic impedance of Z_{03} in this case is 113Ω . The width of this transmission line section in this case would be about $120\ \mu\text{m}$. This corresponds to the limiting value for fabrication process. Thus, lower power division ratios could not be directly implemented. This explains why previously published feeding networks used large values of B in the distribution network to avoid small power division ratios.

In addition, the feeding network in [12] is based on corporate feeding configuration. This configuration cannot be implemented for dual polarizations on the same layer. Thus, this corporate feeding network was implemented on multi-layered strip line configuration which increases the cost and the complexity of the fabrication process.

The proposed feeding network in this paper is based on fork type feeding network configuration as shown in Fig. 10. In this case the two networks of the dual polarizations are interlaced on the same layer. Thus, this feeding network structure is composed on a single layer. The values of the distribution functions in the present case would be $B = 0.4$ and $C = 0.6$ which introduce an error function around 1.23 dBi which is less than the error function of previous feeding networks [3], [12 – 13].

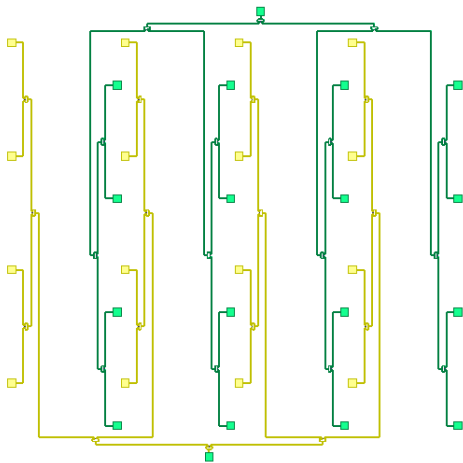


Fig. 10. Fork type dual polarized array feeding network based on Wilkinson power dividers.

Figure 11 shows the proposed distribution function for both amplitude and power ratios. The feeding network consists of four branches. Each two branches are connected by a power divider and these two power dividers are connected by an equal division power divider. On the other hand, each branch consists of four feeding points. Each two feeding points are connected by a power divider and the resulting two power dividers are connected by an equal division power divider. The assumed power division ratio in the first branch is $K_1 = B^2/C^2 = 0.444$, and in the second branch is $K_2 = B^2/A^2 = 0.16$ as shown in Fig. 11. The total normalized power in the first branch is 1.04 and in the second branch is 2.32. Thus, the power division ratio between the first and the second branches is $K_3 = (2B^2 + 2C^2)/(2A^2 + 2B^2) = 0.448$. The first and the third power dividers, K_1 and K_3 , can be fabricated directly with their ratios. However, the second power divider K_2 cannot be fabricated with the present ratio. To implement the power division of K_2 , cascaded power division can be implemented as shown in Fig. 12. In this case, the power between the first and the second feeding points in the second branch is divided by a ratio $K_2 = (B^2 + 0.36)/A^2 = 0.52$. Then this power is divided again between the first feeding point and a matched load by a power division ratio $K'_2 = B^2/0.36 = 0.444$ as shown in Fig. 12. In this case, both power dividers K_2 and K'_2 can be fabricated. However, this additional power divider increases the total normalized power of the second branch to be 3.02. Thus, the power division ratio between the second and the third branch is reduced to be $K_3 = (2B^2 + 2C^2) / (2A^2 + 2B^2 + 0.72) = 0.344$ which cannot be fabricated directly. Thus, the power divider between the two branches should be implemented by cascading two power dividers as in the case of K_2 . This can be done as shown in Fig. 13 where the power divider $K_3 = (2B^2 + 2C^2 + 0.5)/(2A^2 + 2B^2 + 0.72) = 0.51$ is followed by power divider $K'_3 = (2B^2 + 2C^2)/0.5 = 0.48$.

Thus, the final required power dividers have power division ratios $K_1 = K'_2 = 0.444$, $K_2 = 0.52$, $K_3 = 0.51$ and $K'_3 = 0.48$, in addition to equal power dividers. These power dividers are designed by using Keysight ADS2019 and the corresponding designs are verified by using full wave analysis by using Ansoft HFSS. Then, these power dividers are integrated together according to the distribution shown in Fig. 13. Figure 14 shows the geometry of a single arm of the designed fork type feeding network. The ports are arranged from 1 to 17, while the inner numbers in Fig. 14 correspond to the values of the required resistances in Ohms between the arms of the different power dividers. The feeding network shown in Fig. 14 is simulated by using Keysight ADS2019.

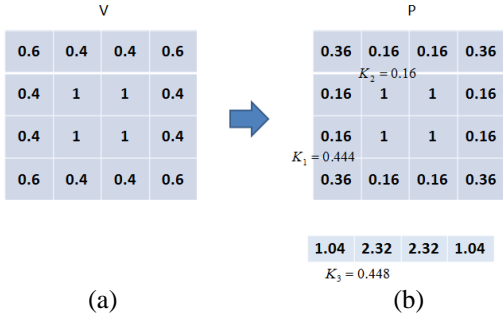


Fig. 11. Proposed feeding distribution: (a) amplitude ratios and (b) power ratios.

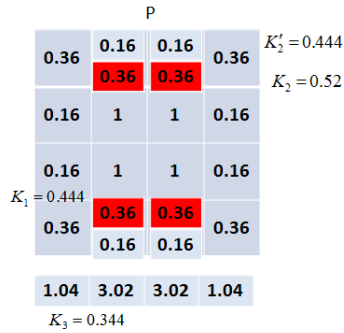


Fig. 12. Power distribution function with cascaded K_2 power division. The red highlighted branches are terminated with matched loads.

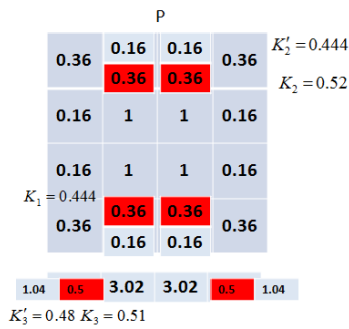


Fig. 13. Power distribution function with cascaded K_2 and K_3 power division. The red highlighted branches are terminated with matched loads.

Figure 15 shows the simulated reflection coefficient of the input port 17. It can be noted that the designed feeding network is good matched below -10 dB reflection coefficient in the operating frequency band from 10.5 to 14.5 GHz.

Figure 16 shows the amplitude ratios of the different output ports with respect to the inner output ports 1-4. It can be noted that the obtained amplitude ratios coincide with the proposed designed values $B = 0.4$ and $C = 0.6$.

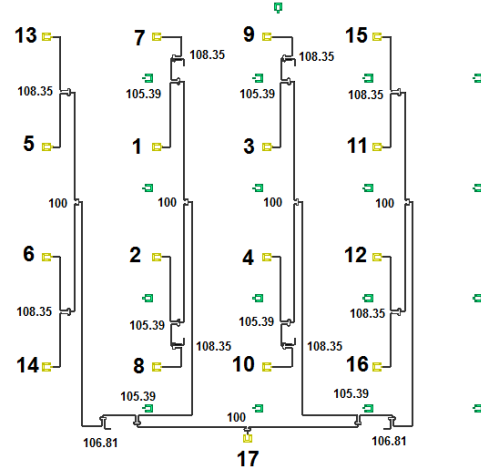


Fig. 14. Geometry of a single arm of the designed fork type dual polarized array feeding network.

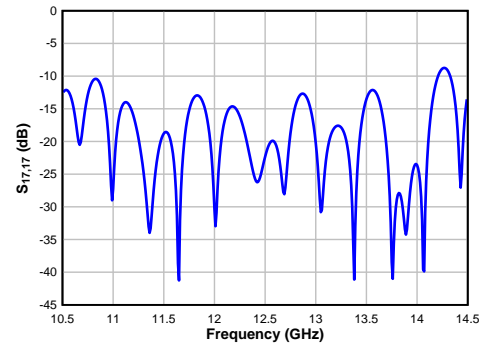


Fig. 15. Simulated reflection coefficient of the input port of the designed fork type feeding network.

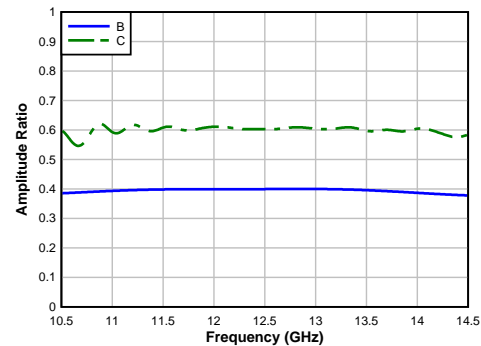


Fig. 16. Simulated amplitude ratios B and C of the designed feeding network.

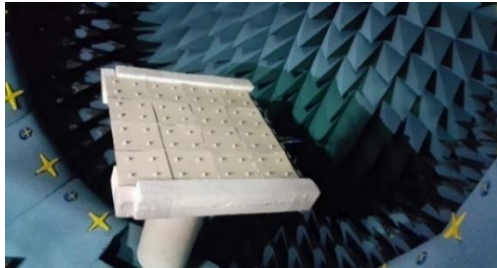
IV. EXPERIMENTAL RESULTS AND DISCUSSIONS

Figure 17 shows the complete fabricated 16×16 antenna array structure including the non-uniform feeding network and the measurement setup inside the anechoic

chamber. The measurements are obtained by using the antenna measurement system Starlab 18 © [21] with a dynamic range of 60dB in the frequency range from 6 to 18 GHz. The antenna is supported by a foam layer with a dielectric constant of about 1.07 which does not have a significant effect on the measured parameters of the fabricated antenna array. The sub-cells are fabricated and assembled separately and the connecting feeding network is fabricated on a separate RO3003 substrate. The sub-cells are connected to the feeding network by using SMP miniaturized push-on connectors on both the sub-cells and the feeding network.



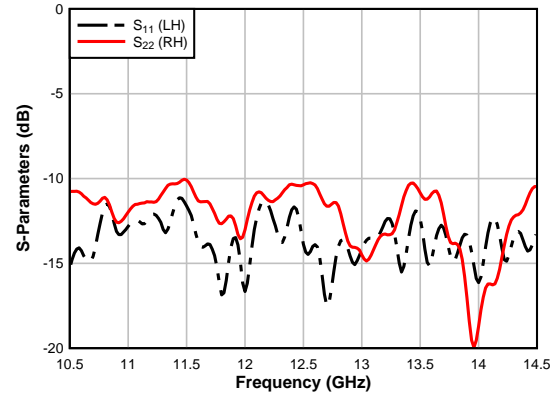
(a)



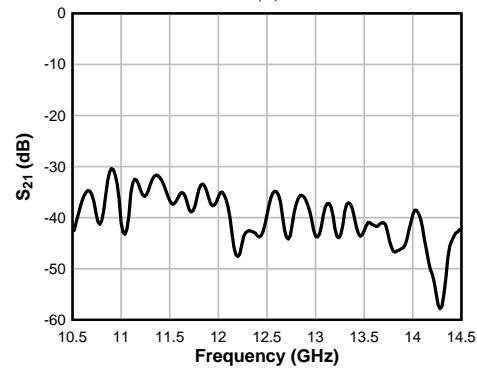
(b)

Fig. 17. Fabricated 16×16 antenna array structure: (a) non-uniform feeding network, and (b) antenna inside the antenna measurement chamber.

Figure 18 (a) shows the measured reflection coefficients of the two feeding ports of the main feeding networks. Port 1 corresponds to the feeding point of LH circular polarization while port 2 corresponds to the feeding point of the RH. It can be noted that good matching is obtained along the required operating bandwidth for both polarizations. On the other hand, Fig. 18 (b) shows the isolation between the two feeding ports. It can be noted that the obtained isolation is less than -30dB over the entire operating bandwidth which is sufficient for the proposed application.



(a)



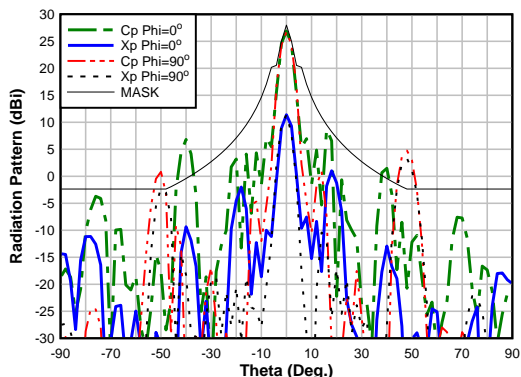
(b)

Fig. 18. Measured S-parameters of the complete antenna structure: (a) measured reflection coefficients of the complete antenna structure for the two feeding ports, and (b) measured isolation between the two feeding ports.

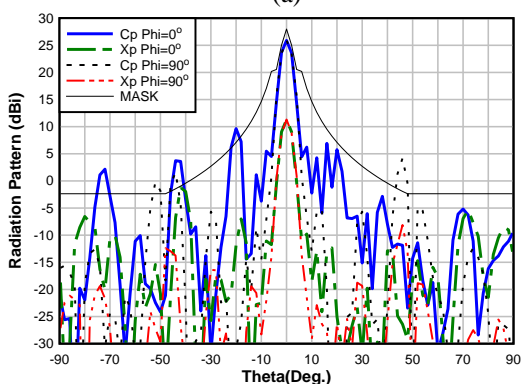
On the other hand, Fig. 19 shows the measured radiation patterns for both LH and RH polarizations compared to the ITU Mask at 12.7 GHz. It can be noted that the obtained radiation patterns are satisfying the ITU Mask except at few separated angles. These are expected results because the proposed feeding distribution does not completely have zero the error function of the simulated radiation pattern with respect to the ITU Mask. In a similar way, Fig. 20 shows the radiation patterns at 11 GHz near the low frequency limit and Fig. 21 shows the radiations patterns at 14 GHz near the upper frequency limit. It can be noted that these radiation patterns also satisfy the required ITU Mask except at few separated angles.

Figure 22 shows the measured peak antenna gain for the two feeding ports while Fig. 23 shows the corresponding axial ratios in the broadside direction. It can be noted that the axial ratio is almost less than 3dB in the required frequency band. Based on the measurement results it can be concluded that the designed non-uniform feeding network for the sub-cells introduces the required radiation parameters for the proposed antenna for on-

move satellite communication system in Ku-band from 10.5 to 14.5 GHz.

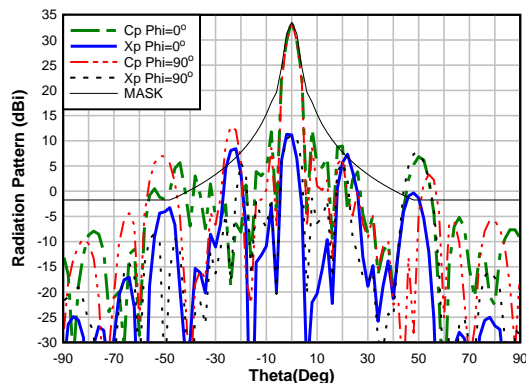


(a)

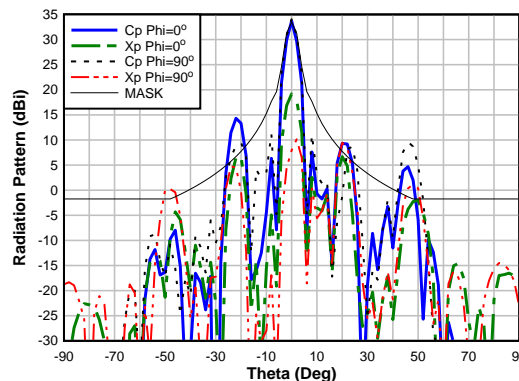


(b)

Fig. 19. Measured radiation patterns compared to the ITU Mask at the planes $\phi = 0^\circ$ and $\phi = 90^\circ$; at 12.7GHz: (a) (Port 1) LH excitation, and (b) (Port 2) RH excitation.

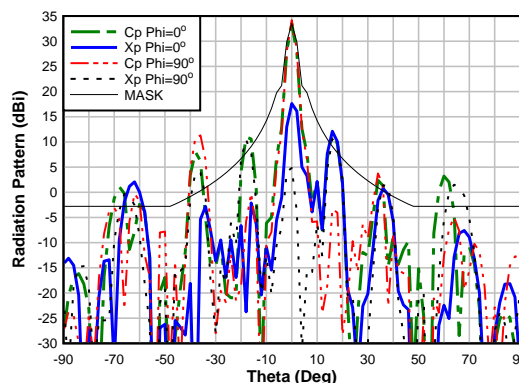


(a)

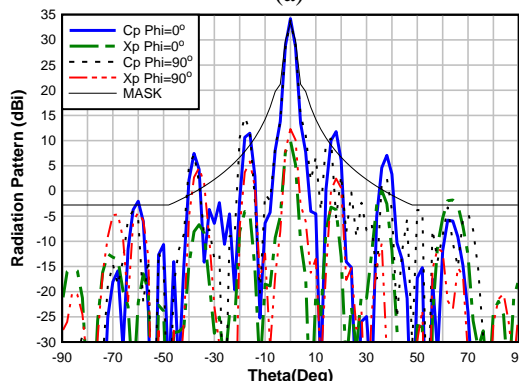


(b)

Fig. 20. Measured radiation patterns compared to the ITU Mask at the planes $\phi = 0^\circ$ and $\phi = 90^\circ$; at 11GHz: (a) (Port 1) LH excitation, and (b) (Port 2) RH excitation.



(a)



(b)

Fig. 21. Measured radiation patterns compared to the ITU Mask at the planes $\phi = 0^\circ$ and $\phi = 90^\circ$; at 14GHz: (a) (Port 1) LH excitation, and (b) (Port 2) RH excitation.

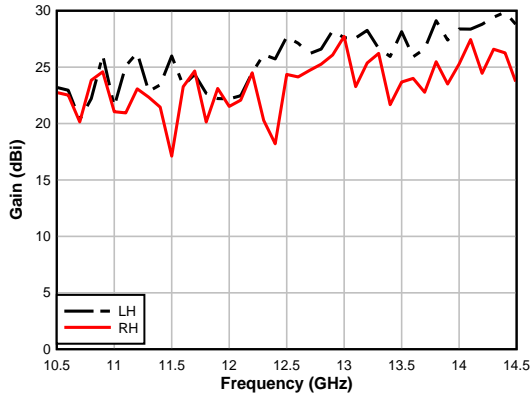


Fig. 22. Measured peak antenna gains for the two feeding ports.

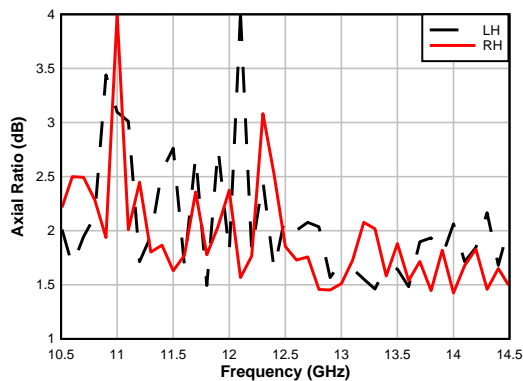


Fig. 23. Measured axial ratios for the two feeding ports.

V. CONCLUSION

Analysis and design of a single layer dual feeding networks for 16×16 Ku band dual circularly polarized antenna array is presented. The antenna array is divided into sub-cells composed of 4×4 radiating elements and connected by a dual sequential feeding network. These sub-cells are connected by a dual non-uniform interlaced fork type feeding networks. New feeding distribution is used to minimize the error between the obtained radiation pattern and the required ITU Mask. The feeding distribution function is verified by using cascaded power dividers to obtain the required small power division ratios. The obtained experimental results satisfy the required properties for a Ku band antenna array for on-move satellite communication system.

REFERENCES

[1] S. K. Lin and Y.-C. Lin, "A compact sequential-phase feed using uniform transmission lines for circularly polarized sequential-rotation arrays," *IEEE Trans. on Antennas Propag.*, vol. 59, no. 7, pp. 2721-2724, July 2011.

[2] "Methods for the determination of the coordination

area around an earth station in frequency bands between 100 MHz and 105 GHz," *2016 Edition of ITU Radio Regulations*, vol. 2, Appendix 7, 2016.

- [3] T. Sallam and A. M. Attiya, "Different array synthesis techniques for planar antenna array," *J. Applied Computational Electromagnetics Society*, vol. 34, no. 5, pp. 716-723, May 2019.
- [4] J. Huang, F. Qiu, W. Lin, Z. Tang, D. Lei, M. Yao, Q.-X. Chu, and Y. J. Guo, "A new compact and high gain circularly-polarized slot antenna array for Ku-band mobile satellite TV reception," *IEEE Access*, vol. 5, pp. 6707-6714, 2017.
- [5] J. Huang, W. Lin, F. Qiu, C. Jiang, D. Lei, and Y. J. Guo, "A low profile, ultra-lightweight, high efficient circularly-polarized antenna array for Ku band satellite applications," *IEEE Access*, vol. 5, pp. 18356-18365, 2017.
- [6] J. Zhu, Y. Yang, S. Li, S. Liao, and Q. Xue, "Dual-band dual circularly polarized antenna array using FSS-integrated AMC ground for vehicle satellite communications," *IEEE Trans. Veh. Technol.*, 2019.
- [7] M. Akbari, A. Farahbakhsh, and A.-R. Sebak, "Ridge gap waveguide multilevel sequential feeding network for high-gain circularly polarized array antenna," *IEEE Trans. on Antennas Propag.*, vol. 67, no. 10, pp. 251-259, Jan. 2019.
- [8] R. Kazemi, S. Yang, S. H. Suleiman, and A. E. Fathy, "Design procedure for compact dual-circularly polarized slotted substrate integrated waveguide antenna arrays," *IEEE Trans. on Antennas Propag.*, vol. 67, no. 6, pp. 3839-3852, June 2019.
- [9] H.-T. Zhang, W. Wang, M.-P. Jin, and X.-P. Lu, "A dual-polarized array antenna for on-the-move applications in Ku-band," *IEEE-APS Topical Conference on Antennas and Propagation in Wireless Communications (APWC)*, pp. 5-8, 2016.
- [10] H.-T. Zhang, W. Wang, M.-P. Jin, Y.-Q. Zou, and X. Liang, "A novel dual-polarized waveguide array antenna for ku band satellite communications," *IEEE International Symposium on Antennas and Propagation & USNC/URSI National Radio Science Meeting*, pp. 633-634, 2017.
- [11] M. M. Bilgic and K. Yegin, "Low profile wideband antenna array with hybrid microstrip and waveguide feed network for Ku band satellite reception systems," *IEEE Trans. on Antennas Propag.*, vol. 62, no. 4, pp. 2258-2263, Apr. 2014.
- [12] A. García-Aguilar, J. M. Inclán-Alonso, L. Vigil-Herrero, J. M. Fernández-González, and M. Sierra-Pérez, "Printed antenna for satellite communications," *IEEE International Symposium on Phased Array Systems and Technology*, pp. 529-535, 2010.
- [13] A. Garcia-Aguilar, J.-M. Inclán-Alonso, L. Vigil-Herrero, J.-M. Fernández-González, and M. Sierra-Pérez, "Low-profile dual circularly polarized

antenna array for satellite communications in the X band,” *IEEE Trans. on Antennas Propag.*, vol. 60, no. 5, pp. 2276-2284, May 2012.

- [14] Y. Q. Zou, H.-T. Zhang, W. Wang, and M.-P. Jin, “Dual circularly polarized waveguide antenna array for satellite communications in the X band,” *IEEE International Symposium on Antennas and Propagation (ISAP)*, pp. 1-3, 2015.
- [15] M. H. Awida and A. E. Fathy, “Substrate-integrated waveguide Ku-band cavity-backed 2×2 microstrip patch array antenna,” *IEEE Antennas and Wireless Propagation Letters*, vol. 8, pp. 1054-1056, 2009.
- [16] A. Harrabi, T. Razban, Y. Mahe, L. Osman, and A. Gharsallah, “Theoretical approach for the design of a new wideband Ku-band printed antenna,” *J. Applied Computational Electromagnetics Society*, vol. 30, no. 11 pp. 1200-1208, 2015.
- [17] S. Trinh-Van, H. B. Kim, G. Kwon, and K. C. Hwang, “Circularly polarized spidron fractal slot antenna arrays for broadband satellite communications in Ku-band,” *Progress in Electromagnetics Research*, vol. 137, pp. 203-218, 2013.
- [18] M. Qu, L. Deng, M. Li, L. Yao, and S. Li, “Compact sequential feeding network with quadruple output ports and its application for wideband circularly polarized antenna,” *IEEE Access*, vol. 6, pp. 31891-31898, Apr. 2018.
- [19] S. Sun, Y. Lv, J. Zhang, Z. Zhao, and F. Ruan, “Optimization based on genetic algorithm and HFSS and its application to the semiautomatic design of antenna,” *IEEE International Conference on Microwave and Millimeter Wave Technology*, pp. 892-894, 2010.
- [20] D. M. Pozar, *Microwave Engineering*. Wiley, 2012.
- [21] https://www.mvg-world.com/en/system/files/starlab_2014.pdf
- [22] K. M. Ibrahim, W. M. Hassan, E. A. Abdallah, and A. M. Attiya, “Wideband sequential feeding network for Ku-band dual circularly polarized 4 × 4 antenna array,” *Int. J. RF Microw. Comput. Aided Eng.*, 2020; e22283. <https://doi.org/10.1002/mmce.22283>



techniques, scattering problems, DRA, transmitarray,

Walaa M. Hassan B.Sc., M.Sc., and Ph.D. degrees from Menoufia University in 2002, 2010 and 2016. She is currently a Researcher at Electronics Research Institute (ERI), Microwave Department, Egypt. Her research interest at, FDFD, breast cancer detection, optimization

reflectarray, solar cell, textile antenna, graphene, and RFID.



Khalid M. Ibrahim B.Sc., M.Sc., and Ph.D. Electronics and Electrical Communications, Faculty of Engineering, Al-Azhar University at 2000, 2007, and 2014 respectively. He joined Electronics Research Institute as a Researcher Assistant in 2001. His research interests include antennas, electromagnetic waves, antennas and wave propagations, ground penetrating radars, antenna and microwave measurement techniques, numerical techniques in electromagnetics.



Esmat A. Abdallah graduated from the Faculty of Engineering and received the M.Sc. and Ph.D. degrees from Cairo University, Giza, Egypt, in 1968, 1972, and 1975, respectively. She was nominated as Assistant Professor, Associate Professor and Professor in 1975, 1980, and 1985, respectively. She has focused her research on microwave circuit designs, planar antenna systems, and recently on EBG structures, UWB components, and antenna and RFID systems. She has authored and coauthored more than 250 research papers in highly cited international journals and in proceedings of international conferences in her field, such as IEEE Transactions on Antenna and Propagation and IEEE Transactions on Microwave Theory Techniques, etc. She supervised more than 70 Ph.D. and M.Sc. thesis. She has been the President of the Electronics Research Institute in Egypt for more than ten years.



Ahmed M. Attiya M.Sc. and Ph.D. Electronics and Electrical Communications, Faculty of Engineering, Cairo University at 1996 and 2001 respectively. He joined Electronics Research Institute as a Researcher Assistant in 1991. In the period from 2002 to 2004 he was a Postdoc in Bradley Department of Electrical and Computer Engineering at Virginia Tech. In the period from 2004 to 2005 he was a Visiting Scholar in Electrical Engineering Dept. in University of Mississippi. In the period from 2008 to 2012 he was a Visiting Teaching Member in King Saud University. He is currently Full Professor and the Head of Microwave Engineering Dept. in Electronics Research Institute. He is also the Founder of Nanotechnology Lab. in Electronics Research Institute.